

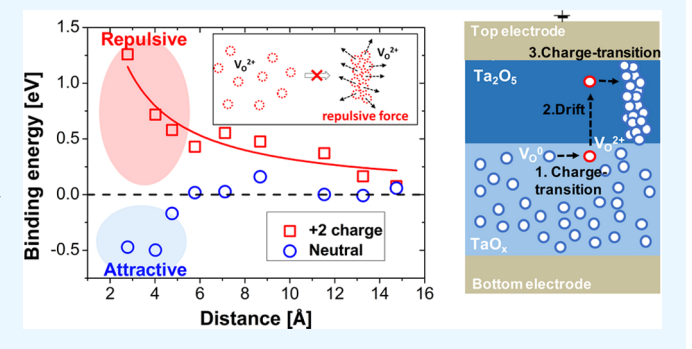
Charge Transition of Oxygen Vacancies during Resistive Switching in Oxide-Based RRAM

Jihang Lee, †, † William Schell, † Xiaojian Zhu, † Emmanouil Kioupakis, *, † and Wei D. Lu*, †

[†]Department of Electrical Engineering and Computer Science and [‡]Department of Materials Science and Engineering, University of Michigan, Ann Arbor, Michigan 48109, United States

Supporting Information

ABSTRACT: Resistive random-access memory (RRAM) devices have attracted broad interest as promising building blocks for high-density nonvolatile memory and neuromorphic computing applications. Atomic level thermodynamic and kinetic descriptions of resistive switching (RS) processes are essential for continued device design and optimization but are relatively lacking for oxide-based RRAMs. It is generally accepted that RS occurs due to the redistribution of charged oxygen vacancies driven by an external electric field. However, this assumption contradicts the experimentally observed stable filaments, where the high vacancy concentration should lead to a strong Coulomb repulsion and filament instability. In this



work, through predictive atomistic calculations in combination with experimental measurements, we attempt to understand the interactions between oxygen vacancies and the microscopic processes that are required for stable RS in a Ta₂O₅-based RRAM. We propose a model based on a series of charge transition processes that explains the drift and aggregation of vacancies during RS. The model was validated by experimental measurements where illuminated devices exhibit accelerated RS behaviors during SET and RESET. The activation energies of ion migration and charge transition were further experimentally determined through a transient current measurement, consistent with the modeling results. Our results help provide comprehensive understanding on the internal dynamics of RS and will benefit device optimization and applications.

KEYWORDS: RRAM, charge transition, vacancy interaction, Ta₂O₅, light illumination

■ INTRODUCTION

Nanoscale memristive devices (RRAM/memristors) have recently attracted significant interest as promising candidates for memory and computing applications due to their simple, two-terminal structure that leads to high integration density 1and the ability to modulate and retain their internal state variable(s) on demand. 5-7 Specifically, the electrical resistance of RRAM devices can be modulated in situ by an external electric field either abruptly or gradually, making them attractive for digital memory as well as artificial neural network applications that require analog-type switching to emulate synaptic plasticity.

The resistive switching (RS) behaviors originate from the internal, microscopic redistribution of ions in response to an applied electric field, leading to a reconfiguration of the material (e.g., structure, composition, and chemical state) and subsequently the modification of the switching material's chemical composition and physical properties. 4,8,9 Ionic migration that leads to the formation of conductive filaments (CFs) by metal cations (e.g., Ag and Cu ions) has been directly observed using in situ transmission electron microscopy (TEM) in electrochemical metallization memory (ECM) devices. 10-12 Additionally, atomic level dynamics in ECM cells have been systematically studied based on the direct observations of CF growth and cyclic voltammetry measurements, in which kinetic parameters such as the diffusion coefficient and the activation energy were successfully determined. 13,14

On the other hand, it is more challenging to directly observe the temporal CF growth in valence-change memory (VCM, commonly referred as oxide RRAM), normally based on transition metal oxides. Since the mobile species in VCM cells, oxygen vacancies (Vos), are intrinsic defects, these devices pose significant challenges for direct experimental analysis.^{4,15} Several theoretical studies have been performed to analyze the RS process in oxide RRAMs, 16-18 although comprehensive atomistic models on internal dynamics during RS have been lacking. Specifically, there appear to be contradictions in the general description of the microscopic processes in RS. For example, oxygen vacancies involved in RS are generally considered as a positively charged $({V_0}^{2+})$ to explain the electric field-driven RS process (i.e., field-driven V_0^{2+} drift).¹⁹ However, in this case, a strong repulsive electrostatic force between charged oxygen vacancies is expected, especially in

Received: November 7, 2018 Accepted: February 28, 2019 Published: February 28, 2019



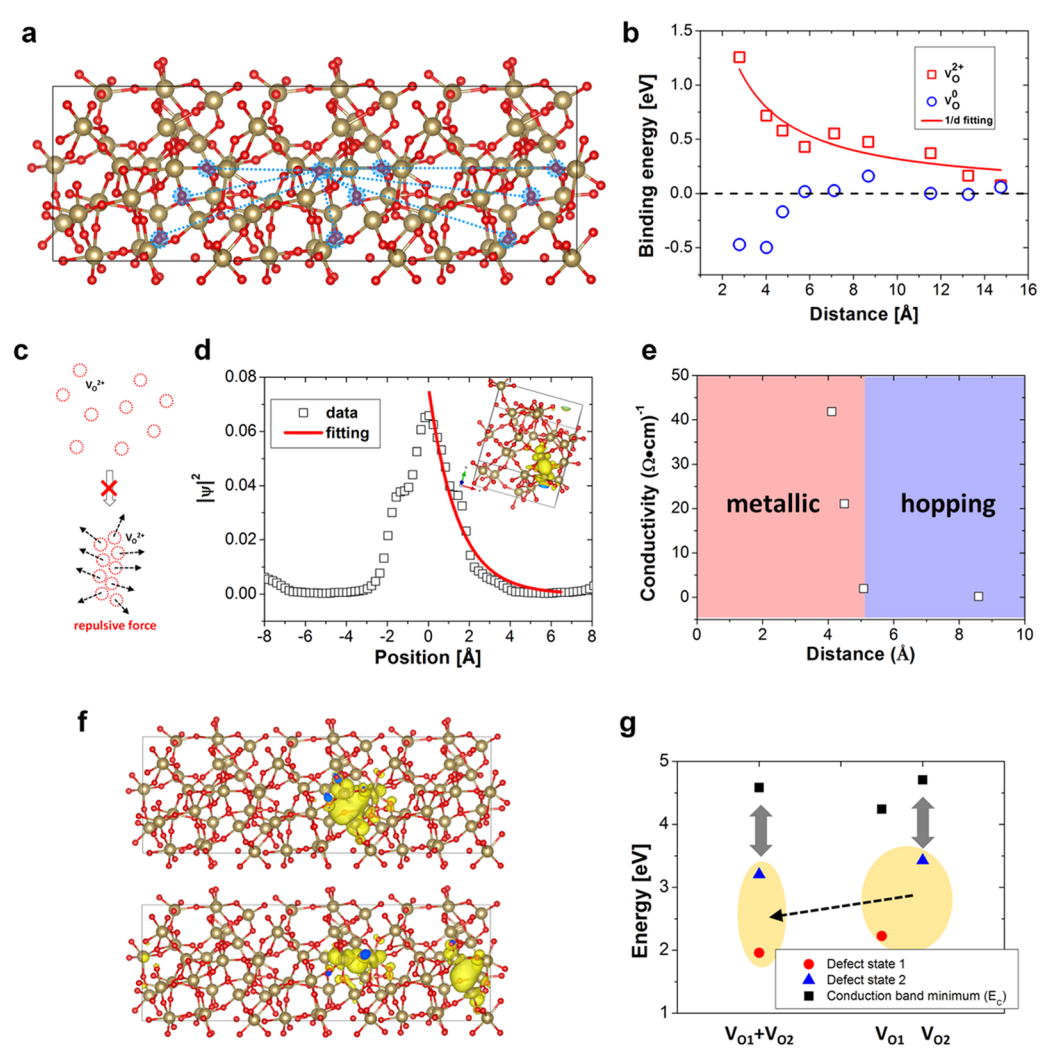


Figure 1. (a) Atomistic configuration of an amorphous-Ta₂O₅ supercell used to study the interactions of oxygen vacancy pairs through DFT calculations. Tantalum and oxygen atoms are represented by gold and red spheres, respectively. The investigated interactions between vacancy pairs at different distances are indicated by cyan circles and dashed lines. (b) The calculated binding energy of oxygen vacancy pairs as a function of the distance. Charged vacancies show a strong Coulomb repulsion, whereas neutral vacancies exhibit a short-range attractive interaction. (c) A schematic illustration of the repulsive interaction between charged vacancies, preventing their aggregation to form a stable CF. (d) Charge density profile of a neutral oxygen vacancy as a function of the distance from the vacancy site, fitted with a decaying exponential function with a characteristic decay length of 2.4 ± 0.4 Å. Inset: charge distribution of the V_O defect state. (e) Experimentally measured conductivity of tantalum oxide films of different stoichiometry (data from ref 25) as a function of distance between vacancies, showing different conduction mechanisms (metallic vs hopping). The transition between the two mechanisms occurs at a vacancy distance of ~5 Å, which is similar to the size of the V_O wave function. Reproduced with permission from ref 25. Copyright 2008 IEEE. (f) Charge distribution of oxygen vacancy pairs with different distances. Top: 2.7 Å and bottom: 13.2 Å. A significant overlap between the two V_O orbitals is observed for the short-distance pair, leading to hybridization. (g) Energy levels of defect states of an oxygen vacancy dimer (V_{O1} + V_{O2}) and of two isolated vacancies, showing the lowering of two occupied defect states due to the hybridization and interaction with the conduction band. The energy levels are referenced to the valence band maximum.

filaments where the concentration of oxygen vacancies is very high. This, in turn, contradicts the experimentally observed long retention and excellent stability of CFs in oxide-based RRAM. Developing an atomistic picture that can comprehensively explain the internal dynamics of RS in oxide-based RRAM thus becomes critical to improving the understanding of RS processes and guide continued device optimization and

In this work, we investigate the interactions between oxygen vacancies in different charge states in an amorphous Ta2O5 cell, shown in Figure 1a, using first-principles calculations based on density functional theory (DFT) implemented in the Vienna ab initio simulation package (VASP).20 We find a strong repulsive interaction between charged vacancies,

whereas neutral vacancies experience short-range attraction. Based on our theoretical predictions, we propose a model consisting of a series of charge transition processes that successfully explains the drift and aggregation of vacancies during RS. Our model reconciles experimental observations, including the field-driven ionic transport and the formation of stable filaments with high V_O concentration. We further validate the model with electrical measurements. Our results show accelerated resistive switching behavior and lower activation energy under visible-light illumination, which can be ascribed to the enhanced charge transition of oxygen vacancies under light illumination.

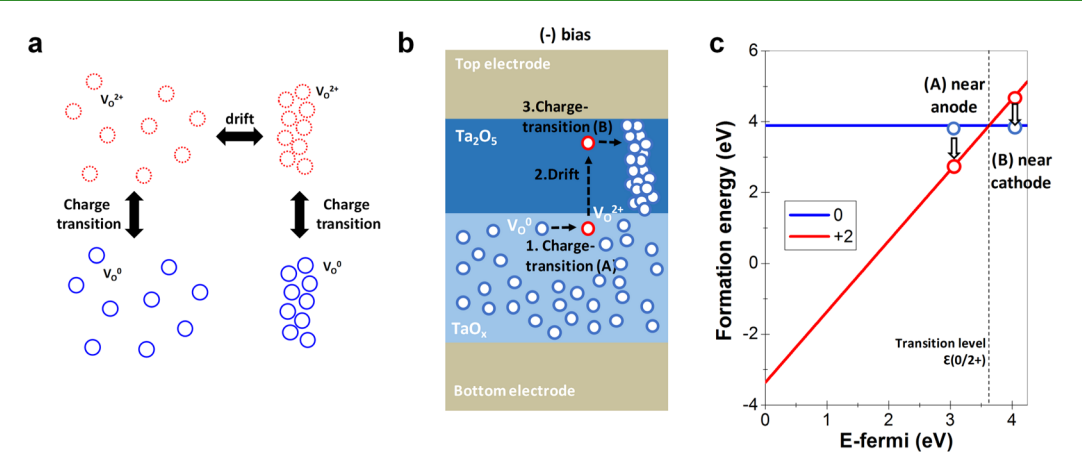


Figure 2. (a) Schematic of the proposed charge transition and migration processes of oxygen vacancies during RS. (b) Illustration of the formation of a CF including the charge transition processes and ionic migration in a bilayer Ta_2O_5 -based RRAM device. (c) Formation energy of an oxygen vacancy (neutral and +2 charged states) in amorphous Ta_2O_5 as a function of the Fermi level.³⁴ Reproduced with permission from ref 34. Copyright 2017 The Royal Society of Chemistry. Neutral vacancies near the anode can transit to the charged state (A), followed by a drift toward the cathode. The charged vacancies convert back to the neutral state as they approach the cathode due to the increased E_{Fermi} (B) under negative bias on the cathode.

RESULTS AND DISCUSSION

The details of our DFT calculations can be found in the Supporting Information. Specifically, the binding energy of oxygen vacancy pairs (i.e., the difference between the formation energy of a vacancy dimer and two isolated vacancies) at different distances, as indicated in Figure 1a, was calculated by the following equation ^{17,21}

$$E_{\text{binding}}(q) = E^{f}[V_{O_{1}}^{q} + V_{O_{2}}^{q}] - (E^{f}[V_{O_{1}}^{q}] + E^{f}[V_{O_{2}}^{q}])$$
(1)

where E^{t} is the formation energy of oxygen vacancies (see eq S1 in the Supporting Information) and *q* is their charge state. The calculated binding energy as a function of distance between two vacancies is shown in Figure 1b. First, we found that the binding energy of vacancy pairs in the +2 charge state is positive, consistent with previous calculations in TiO₂, ^{17,22} and also increases with decreasing distance, indicating the expected strong repulsive interaction between charged vacancies. The repulsive energy is inversely proportional to the distance between the charged vacancies (V_O²⁺s), consistent with electrostatic Coulombic repulsion between charged particles. It should be noted that although the repulsive interaction between charged vacancies becomes negligible at distances larger than ~13 Å, the estimated distance between oxygen vacancies in CFs is typically much shorter. For example, Chen et al. reported an O/Ta ratio of ~2:1 in the filament region in amorphous Ta2O5-based RRAM devices from cross-sectional TEM and energy dispersive X-ray spectroscopy (EDS) analysis, 23 which corresponds to a high $m V_{O}$ concentration with a distance between vacancies of \sim 5 Å in the filament region. Therefore, a strong repulsive force should exist between charged V_O²⁺s in CFs for typical vacancy concentrations, potentially preventing vacancies from aggregating and forming stable CFs, as illustrated in Figure 1c. This contradicts the experimentally observed stable CFs in Ta₂O₅based RRAM devices with long retention at high Vo concentration conditions.^{3,24}

On the other hand, our calculations show that neutral oxygen vacancies (V_0^0) exhibit short-range attraction with a negative binding energy, 17,22 as shown in Figure 1b. To understand the driving force of the attractive interaction

between neutral vacancies, we determined the localization length of electrons in occupied midgap states from neural vacancies. Our results show that electrons bound to neutral vacancies are highly localized and their charge density decreases exponentially with increasing distance from the vacancy, as shown in Figure 1d, with a localization length of 2.4 ± 0.4 Å. The diameter of the V_{O} wave function in amorphous Ta₂O₅ is remarkably consistent with the critical V_O distance for the transition between metallic and hopping conductions in Ta2O5 RRAM devices from experimental conductivity measurements.²⁵ Specifically, we plotted the experimentally measured conductivity of tantalum oxide films with different stoichiometry, 25 as a function of VO concentration (Figure S1) and correspondingly the V_O distance (Figure 1e). Here, we note that tantalum oxide films with different stoichiometry were considered as amorphous Ta2O5 films having various VO concentrations, because Ta2O5 is the solely stable phase in Ta-O system, whereas substoichiometric phases are not thermodynamically stable according to the phase diagram. In the regime of high V_O concentration (>7 \times 10²¹ cm⁻³), the conductivity of Ta₂O₅ films increases linearly with increasing V_O concentration, whereas the trend of conductivity below the critical concentration N_C exhibits not a linear but an exponential dependence, indicating metallic and hopping conduction mechanisms in these two regimes, respectively.^{3,26,27} The corresponding critical distance (~5 Å) of V_O s at the critical V_O concentration N_C is in very good agreement with the calculated size of the $V_{\rm O}$ wave function in our study and also agrees with the experimentally estimated V_O distance in a stable CF based on EDS analysis.²³ These agreements reveal the change of the conduction mechanism during RS in Ta₂O₅ devices. Specifically, metallic conduction of the on-state is caused by continuous overlapping of the localized electron states induced by V_O (as defects), where the $V_{\rm O}$ distance is shorter than the size of the $V_{\rm O}$ wave function, thus creating electronic conduction paths connecting one electrode to the other. During the reset process, V_O migration reduces the V_O concentration and leads to an increased V_O distance, resulting in a reduced electron overlap. As a result, electrical conduction in the off-state is dominated by the hopping mechanism with a lower conductivity.

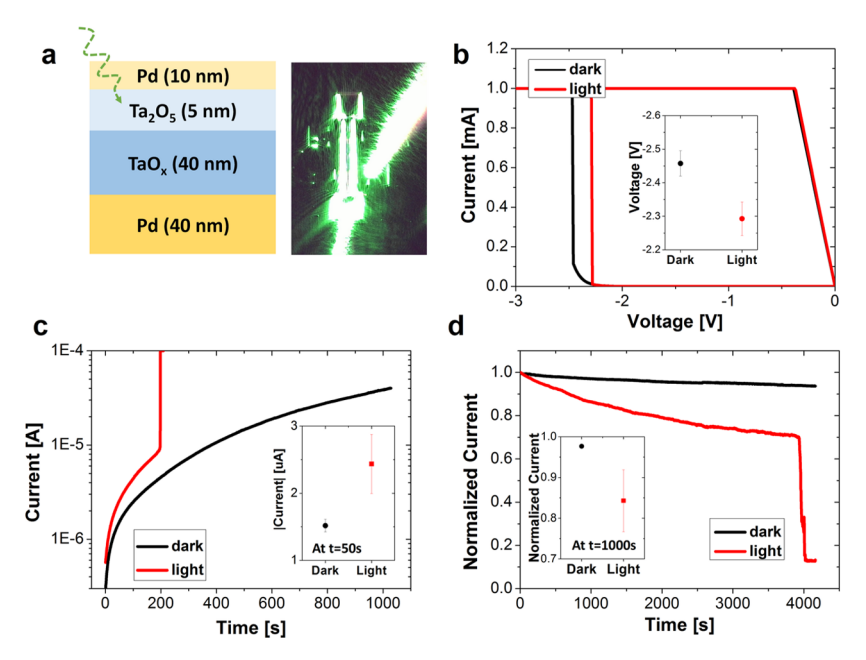


Figure 3. (a) Schematic of a Ta₂O₅-based bilayer device structure with a thin top electrode to enable light illumination on the switching layer (left), and optical-microscope image of the device illuminated by a green-light laser during electrical measurements (right). (b) Direct current I-Vcharacteristics during the electroforming process with and without light illumination. Inset: average and standard deviation of the forming voltage measured from multiple devices under light and dark conditions. (c) Current evolution of as-fabricated devices under constant voltage stress (-2 V), with and without light illumination. Inset: current level of the devices after 50 s under the constant bias. (d) The current evolution of devices in LRS under constant erasing voltage stress (0.8 V). Inset: current level after 1000 s under the constant bias.

The short-range attractive interaction between neutral vacancies (Figure 1b) can be explained by the hybridization of overlapping electron states.^{28,29} The overlap of two electron states localized at different neutral oxygen vacancy sites (Figure 1f, top panel) gives rise to two midgap defect states that are lower in energy compared to those of isolated vacancies (Figure 1g). The lower-V_O level moves downward as a result of hybridization between the two defect orbitals,²⁹ whereas the upper-V_O level is also pushed down due to repulsion by the conduction band. Consequently, both occupied defect levels become lowered in energy, leading to a negative binding energy and attractive interaction at vacancy-vacancy distances shorter than the size of neutral vacancy orbitals. We believe that this attractive interaction facilitates the aggregation of vacancies and the formation of stable CFs with high V_O concentration during RS.

On the other hand, even though neutral vacancies can explain the aggregation and the formation of stable CFs, their charge neutrality precludes the field-driven drift, as observed during RS. To resolve these contradictions, we consider a series of charge transition processes during the RS process, which enables both the field-driven VO drift and allows stable Vo aggregation. Figure 2a shows a schematic of the proposed charge transition and drift processes that result in CF formation/rupture during RS. Note that the formation energy of charged defects (e.g., V_0^{2+}) depends on the Fermi level, and that the formation energy of neutral vacancy lies within the range of the charged ${\rm V_O}^{2+}$ formation energy between the cases that the Fermi level is near the valence band maximum (E_V) and near the conduction band minimum (E_C) , as shown in Figure 2c. As a result, the stable V_O charge state can change between neural $V_O^{\ 0}$ and charged $V_O^{\ 2+}$, depending on the Fermi level, which is in turn affected by the applied voltage during the device operation. For example, the lower Fermi level near the anode stabilizes the +2 charge state, whereas the neutral charge

state becomes more stable near the cathode due to the elevated Fermi level.

Figure 2b shows how isolated oxygen vacancies aggregate and form a CF during RS, along with changes of the relative stability between neutral and charged vacancies. Starting from the neutral charge state, isolated V_O⁰s become ionized into ${
m V_O}^{2+}$ s near the anode with lower Fermi level. Then, the charged V_0^{2+} s migrate toward the cathode through the fielddriven drift process and accumulate there in which the applied electric filed enables ${\rm V_O}^{\rm 2+}{\rm s}$ to overcome the repulsive force during programming. As more ${\rm V_O}^{2+}$ s accumulate near the cathode and the V_O concentration increases, the Fermi level rises, leading to another charge transition from +2 to the neural state (Figure 2b). As a result, a stable CF consisting of aggregated V_0^0 s is formed without repulsive interactions. On the other hand, if the applied field is removed without the subsequent charge transition process, the formed CF (consisting of V_O²⁺s) will become unstable. Therefore, this model can explain the experimentally observed excellent retention of Ta₂O₅-based devices at high V_O concentration, ^{24,30} providing an atomistic picture on the stability of CFs during RS and offering design guidelines to achieve desirable device properties such as long retention. For example, retention failure can occur when oxygen vacancies diffuse out from the CF by overcoming both the migration barrier and the binding energy due to vacancy interactions. Indeed, the experimentally measured vacancy diffusion activation energy is 1.6 eV through retention tests, 24 which is larger than the value of 1.2 eV obtained from profiling oxygen concentration during annealing in which diffusion is due to noninteracting vacancies.31 This discrepancy can be explained by the increased barrier height in the filament due to the attractive interaction energy. Therefore, resistive switching devices with long retention (where the activation energy is determined by interacting vacancies) and low programming voltage (where

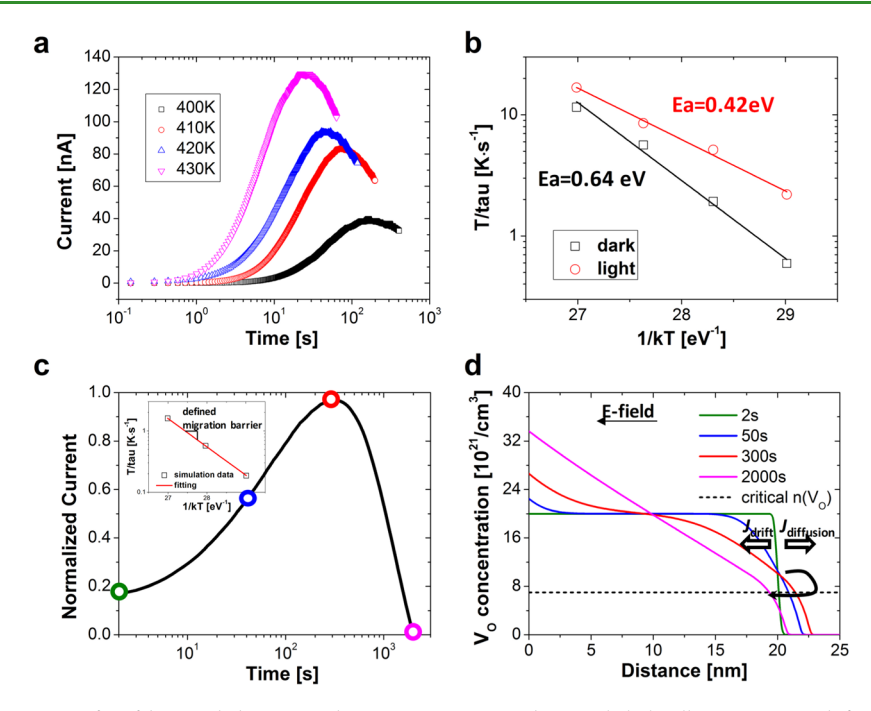


Figure 4. (a) I-t characteristics of as-fabricated devices under constant positive bias with light illumination at different temperatures, showing transient current peaks. (b) The Arrhenius plot of the transient current peaks, showing lower activation energy under illumination. (c) Simulated I-t characteristics showing a transient current peak. Inset: Arrhenius plot of the current peak position obtained from the simulation vs temperature. The activation energy extracted from this method is indeed the migration barrier used in the numerical simulation setup. (d) Simulated V_O concentration profile at each stage indicated in (c). The conductive region initially expands and subsequently contracts, leading to an increase and decrease of the device conductance and the observed current peak.

the migration of vacancies is determined by noninteracting vacancies) can be achieved by utilizing defects with short-range attractive interactions.

To test the hypothesis of charge transition of oxygen vacancies during RS in oxide-based RRAM, we designed an experiment that employs visible-light illumination to control the V_O charge state. Specifically, electrons trapped at the midgap defect states of V_O⁰ can be excited into the conduction band by light absorption, inducing a charge transition from 0 to +2 state. For example, it has been reported that V_O migration in SrTiO3 is accelerated by visible-light illumination due to the photoexcitation of midgap states, where $V_{\rm O}^{\ 1+}$ s in the form of Ti-V_O complexes are ionized to V_O²⁺s with a lower activation energy for ionic migration.³² In our experiment, we employed green light (520 nm) whose photon energy is larger than the absorption energy of oxygen vacancies in Ta₂O₅ but smaller than the Ta₂O₅ band gap. 33,34 As a result, the characteristics of RS behaviors in Ta2O5-based RRAM devices would be affected by visible-light illumination if the charge transition processes are indeed involved in the RS. Figure 3a shows the structure of a Ta2O5-based bilayer device used in this study, where a thin (10 nm) Pd top electrode (TE) was used to allow light pass through onto the switching layer. Devices with the thin TE are still fully functional and show reliable RS characteristics that are almost identical to standard devices with thick TE (Figure S2). A device being illuminated by a green-light laser (520 nm) during electrical measurements is shown in Figure 3a.

The effects of light illumination on the RS behavior were first examined in the electroforming process. As shown in Figures 3b and S3, illuminated devices show a smaller forming voltage at which the device conductance abruptly increases from the highly resistive virgin state. For example, the average

forming voltage for the illuminated devices is -2.3 ± 0.05 V, which is smaller than that of unilluminated devices, -2.45 ± 0.04 V. To more clearly illustrate the light-induced effects, devices in virgin state were subjected to a low voltage (-2 V) stress, where the applied voltage was lower than the typical forming voltage, and the current through the devices was monitored. Figure 3c shows the current evolution for devices with and without light illumination. The average current value for the illuminated device is clearly larger than the dark case, as further verified in the inset of Figure 3c. In addition, an abrupt drop of resistance, corresponding to the electroforming process, occurs only under illumination conditions within our measurement time at this low bias conditions.

Such behavior of the resistance decrease can be well understood in the picture of V_O-migration from the V_O-rich TaO_x layer to the V_O-poor Ta₂O₅ layer during the electroforming process. Since the Ta₂O₅ switching layer is electrically much more resistive than the TaO_x layer, the total device resistance is determined by the V_O concentration in the Ta₂O₅ layer. As charged oxygen vacancies migrate to the switching layer due to field-driven drift under the negative voltage applied to the top electrode, the total resistance of the device is reduced over time. Here, the light illumination speeds up the injection of charged V_O into the switching layer by facilitating the charge transition from $V_O^{\ 0}$ to $V_O^{\ 2+}$. That is, light absorption converts more neutral vacancies to the +2 charged state. It is these charged V_O²⁺s that respond to the applied electric field and migrate into the switching layer, so the higher V_{O}^{2+} concentration due to light-induced charge transition leads to larger conductance increase and reduced electroforming

The effect of visible-light illumination was further investigated in the RESET process. Similarly, a constant voltage (0.8

V), which is lower than the typical RESET voltage, was applied to devices with and without light illumination. Prior to this measurement, the devices were switched to the LRS under dark conditions with similar resistance values. Figure 3d shows the change of the normalized current over time under a constant positive 0.8 V voltage bias, for the illuminated and dark cases. Both cases show the degradation of the LRS current over time. However, the illuminated devices show much faster decay, followed by an abrupt drop of current that corresponds to the breakage of the CF. The inset of Figure 3d shows the average value of current after 1000 s under dark and illuminated conditions from multiple devices, verifying the accelerated erasing process under light illumination. The accelerated RESET transition by visible-light illumination observed here is consistent with a previous work in which the electrical conductivity and the size of a nanoscale CF (formed by a conductive atomic force microscope tip) in HfO₂ became reduced upon white-light illumination.

The accelerated degradation of the LRS under illumination is again attributed to photoinduced charge transition from V₀ to V_{O}^{2+} . In general, the RESET process is believed to be driven by out-diffusion of oxygen vacancies due to Joule heating followed by Vo drift that creates and widens a Vo-depleted gap. 19 However, the applied bias in this measurement itself is not large enough to cause significant diffusion or drift of Vos from the CF. This is consistent with the slow degradation of the conductance observed under dark conditions. On the contrary, light illumination leads to photoexcitation of electrons from the midgap states of $V_{\rm O}{}^{\rm 0}s$. As a result, the aggregated V_0^0 s constituting the CF are transited to V_0^{2+} s that experience strong repulsive interactions, thus accelerating the migration of the vacancies and deteriorating the stability of the CF. Additionally, the light-assisted charge transition to the +2 state causes vacancies to respond to the applied electric field and enables Vo drift. The observed faster RESET under light illumination thus further supports our model of the charge transition processes in oxide RRAM devices.

The activation energies of ion migration and charge transition were then experimentally determined through a transient current measurement. 36,37 Under constant positive bias, the as-fabricated devices exhibited transient current peaks when the current is plotted against time, as shown in Figure 4a. The positions of the transient current peaks can be fitted with the Arrhenius equation, as shown in Figure 4b. We found that illuminated devices exhibit lower activation energy (0.42 eV) than unilluminated devices (0.64 eV), consistent with our experimental results showing the light-induced accelerated RS behaviors (Figure 3). Specifically, since the charge transition from the neutral to the +2 state is facilitated by light absorption, vacancies in an illuminated device are in the charged state, and the estimated value from the transient current measurement is the activation energy for the migration of charged V_O²⁺. Indeed, the experimentally estimated value of the activation energy under light illumination is in very good agreement with the theoretically calculated migration barrier of ${
m V_0}^{2+}$ in ${
m Ta_2O_5}$ (${\sim}0.4$ eV), 38 supporting the charge transition model. On the other hand, the activation energy measured under dark conditions (0.64 eV) should correspond to the charge transition process, since this process requires higher energy and dominates during the measurement of V_O²⁺ drift. We note that the ionization energy of oxygen vacancy (0.6-0.8)eV)34,39,40 is indeed consistent with our experimentally obtained value.

An analytical model that reveals the relation between the peak position from the transient current measurements and the activation energy was developed as described in eq 2

$$\frac{T}{\tau} = \alpha D_0 \exp\left(-\frac{E_a}{kT}\right)$$
, where $\alpha = \frac{qE}{x_c k}$ (2)

where T is absolute temperature, D_0 and E_a are the preexponential constant and the activation energy of V_O diffusion, x_c is the boundary position (measured from the interface) of the conductive region having vacancy concentration above the critical V_O concentration, k and q are the Boltzmann's constant and the charge of the oxygen vacancy, respectively (derivation of eq 2 can be found in eqs S2-S8 in the Supporting Information). Here, the position of the transient current peak (τ) was determined as the time at which the time derivative of the V_O concentration becomes zero, corresponding to when the diffusion and drift fluxes become equal with opposite sign. This analytical model was confirmed through numerical simulations in which the electronic continuity equation, the ionic drift/diffusion equation, and the Fourier equation for Joule heating are self-consistently solved. 19 With a simulation cell including V_O-rich and V_O-poor switching layers, a transient current peak was indeed observed under constant bias, as shown in Figure 4c. The activation energy determined from the peak positions (Figure 4c inset) is indeed the energy barrier for ionic migration used in the simulation, thus validating the results obtained in Figure 4b.

Figure 4d shows the concentration profile at each stage during the transient current measurement (under a constant positive bias on the TE). In the beginning, V_O diffusion is dominant due to the large Vo concentration gradient, driving the boundary at which the V_O concentration is equal to N_C toward the right, and thus leads to the expansion of the conductive region. The length of the conductive region reaches a maximum when the diffusion and drift fluxes become equal, corresponding to the maximum conductance and the observed current peak (the red circle in Figure 4c). Beyond this point, the boundary starts to move toward the left due to the dominating V_O drift term, resulting in a reduction of the conduction region and a decrease of the device conductance and consequently a decrease in current. These microscopic processes explain the transient current peak during constant positive bias as observed in the experiment and numerical simulation.

CONCLUSIONS

In summary, we show that positively charged oxygen vacancies (V_O²⁺) in Ta₂O₅ show a strong mutual repulsion due to electrostatic Coulomb interaction, whereas neutral vacancies exhibit a short-range attractive force that facilitates aggregation to form a stable conductive filament. Neutral vacancies, however, do not produce V_O drift in an applied electric field. We, therefore, propose a model based on a series of charge transition processes to consistently explain both the aggregation and the field-driven drift of oxygen vacancies during RS. Our proposed model is further supported by experimental studies. Specifically, oxide RRAM devices exhibit accelerated switching under illumination due to the lightassisted charge transition of oxygen vacancies, supporting the charge transition model. Furthermore, we experimentally determined the activation energies of the charge transition and the V_O-migration processes based on the transient current measurement. Illuminated devices show an apparent lower activation energy, with an experimentally estimated value in good agreement with the calculated migration barrier of charge vacancies (${\rm V_O}^{2+}$). The development of the transient current peak can be explained by ${\rm V_O}$ drift and diffusion processes, where the dependence of the peak location as a function of temperature was verified by numerical simulations. Our results help provide a understanding of the internal dynamics of resistive switching in oxide RRAM and will help guide device optimization and applications.

■ EXPERIMENTAL SECTION

Computational Calculation. The equilibrium geometry of the atoms, the total energies, and electronic wave functions are obtained using the Vienna ab initio simulation package (VASP) with a planewave cutoff of 400 eV and included the Ta $5s^25p^65d^36s^2$ and O $2s^22p^4$ electrons in the valence. The formation energy of defects was calculated by the following equation 21

$$E^{f}[X^{q}] = E_{tot}[X^{q}] - E_{tot}[bulk] - \sum_{i} n_{i}\mu_{i} + q\mu_{e} + E_{corr}$$
(3)

where $E_{\rm tot}[X^q]$ and $E_{\rm tot}[{\rm bulk}]$ are the total energy of a cell having a defect with charge q and a defect-free bulk cell, respectively. The parameters μ_i and μ_e are the chemical potentials of atoms that are removed ($\mu_i < 0$) or added ($\mu_i > 0$) and the chemical potential of the electron. A large supercell consisting of 252 atoms was employed to investigate a V_O dimer with long distance while minimizing artificial interactions with periodic images in finite-size supercell approach. The binding energy was calculated with the Perdew–Burke–Ernzerhof functional and a 1 \times 1 \times 3 supercell that allows the distance of a vacancy dimer to vary up to 15 Å.

Experimental Method. Ta_2O_5 -based RRAM devices used in this work were fabricated in a crossbar structure. The bottom electrode (Pd, 40 nm) was patterned by photolithography and deposited by an e-beam evaporation and lift-off. Then, a tantalum suboxide (TaO_x) layer (40 nm) was deposited by reactive sputtering using a Ta target with a gas flow of Ar/O_2 (32.3:1), followed by the deposition of a tantalum pentoxide (Ta_2O_5) layer by radio frequency sputtering using a Ta_2O_5 ceramic target without breaking vacuum. Next, the top electrode (Pd, 10 nm) was deposited and patterned as the top electrode followed by reactive ion etching process to open the bottom electrode pads. A green-light laser (520 nm) with a power of 16 mW was employed for the light-illumination experiments.

ASSOCIATED CONTENT

S Supporting Information

The Supporting Information is available free of charge on the ACS Publications website at DOI: 10.1021/acsami.8b18386.

Computational and experimental methods, conductivity of Ta_2O_5 films, I-V characteristics of RS in Ta_2O_5 -based bilayer device, light-accelerated RS behaviors, analytical model for the transient current method (PDF)

AUTHOR INFORMATION

Corresponding Authors

*E-mail: wluee@umich.edu (W.D.L..).

*E-mail: kioup@umich.edu (E.K.).

ORCID ®

Emmanouil Kioupakis: 0000-0003-1880-6443

Wei D. Lu: 0000-0003-4731-1976

Author Contributions

The manuscript was written through contributions of all authors. All authors have given approval to the final version of the manuscript.

Notes

The authors declare no competing financial interest.

ACKNOWLEDGMENTS

The authors would like to thank Y. Jeong, F. Cai, J. Shin, and Dr M. Zidan for helpful discussions. The study was partially supported by the National Science Foundation (NSF) through grants ECCS-0954621 and DMR-1810119. J.L. also acknowledges support by the Rackham Predoctoral Fellowship. The DFT calculations were supported by the National Science Foundation through Grant No. DMR-1810119. Computational resources were provided by the National Energy Research Scientific Computing Center, supported by the Office of Science of the U.S. Department of Energy under contract no. DE-AC02-05CH11231.

REFERENCES

- (1) Yang, J. J.; Pickett, M. D.; Li, X.; Ohlberg, D. A. A.; Stewart, D. R.; Williams, R. S. Memristive Switching Mechanism for Metal/Oxide/Metal Nanodevices. *Nat. Nanotechnol.* **2008**, *3*, 429.
- (2) Waser, R.; Dittmann, R.; Staikov, G.; Szot, K. Redox-Based Resistive Switching Memories Nanoionic Mechanisms, Prospects, and Challenges. *Adv. Mater.* **2009**, *21*, 2632–2663.
- (3) Yang, J. J.; Strukov, D. B.; Stewart, D. R. Memristive Devices for Computing. *Nat. Nanotechnol.* **2013**, *8*, 13–24.
- (4) Lee, J.; Lu, W. D. On-Demand Reconfiguration of Nanomaterials: When Electronics Meets Ionics. *Adv. Mater.* **2018**, *30*, No. 1702770.
- (5) Prezioso, M.; Merrikh-Bayat, F.; Hoskins, B. D.; Adam, G. C.; Likharev, K. K.; Strukov, D. B. Training and Operation of an Integrated Neuromorphic Network based on Metal-Oxide Memristors. *Nature* **2015**, *521*, 61–64.
- (6) Sheridan, P. M.; Cai, F.; Du, C.; Ma, W.; Zhang, Z.; Lu, W. D. Sparse Coding with Memristor Networks. *Nat. Nanotechnol.* **2017**, *12*, 784–789.
- (7) Zidan, M. A.; Strachan, J. P.; Lu, W. D. The Future of Electronics based on Memristive Systems. *Nat. Electron.* **2018**, *1*, 22–29
- (8) Strukov, D. B.; Snider, G. S.; Stewart, D. R.; Williams, R. S. The Missing Memristor Found. *Nature* **2008**, *453*, 80–83.
- (9) Yang, Y.; Lu, W. Nanoscale Resistive Switching Devices: Mechanisms and Modeling. *Nanoscale* **2013**, *5*, 10076–10092.
- (10) Yang, Y.; Gao, P.; Gaba, S.; Chang, T.; Pan, X.; Lu, W. Observation of Conducting Filament Growth in Nanoscale Resistive Memories. *Nat. Commun.* **2012**, *3*, No. 732.
- (11) Yang, Y.; Gao, P.; Li, L.; Pan, X.; Tappertzhofen, S.; Choi, S.; Waser, R.; Valov, I.; Lu, W. D. Electrochemical Dynamics of Nanoscale Metallic Inclusions in Dielectrics. *Nat. Commun.* **2014**, *S*, No. 4232.
- (12) Hubbard, W. A.; Kerelsky, A.; Jasmin, G.; White, E. R.; Lodico, J.; Mecklenburg, M.; Regan, B. C. Nanofilament Formation and Regeneration During Cu/Al₂O₃ Resistive Memory Switching. *Nano Lett.* **2015**, *15*, 3983–3987.
- (13) Valov, I.; Waser, R.; Jameson, J. R.; Kozicki, M. N. Electrochemical Metallization Memories Fundamentals, Applications, Prospects. *Nanotechnology* **2011**, *22*, No. 289502.
- (14) Valov, I.; Lu, W. D. Nanoscale Electrochemistry using Dielectric Thin Films as Solid Electrolytes. *Nanoscale* **2016**, *8*, 13828–13837.
- (15) Yang, Y.; Lu, W. D. Progress in the Characterizations and Understanding of Conducting Filaments in Resistive Switching Devices. *IEEE Trans. Nanotechnol.* **2016**, *15*, 465.
- (16) Xiao, B.; Watanabe, S. Oxygen vacancy effects on an amorphous-TaOx based resistance switch: a first principles study. *Nanoscale* **2014**, *6*, 10169–10178.
- (17) Kamiya, K.; Yang, M. Y.; Park, S.-G.; Magyari-Köpe, B.; Nishi, Y.; Niwa, M.; Shiraishi, K. ON-OFF Switching Mechanism of

- Resistive—Random—Access—Memories based on the Formation and Disruption of Oxygen Vacancy Conducting Channels. *Appl. Phys. Lett.* **2012**, *100*, No. 073502.
- (18) Bondji, R. J.; Marinella, M. J. Oxidation state and interfacial effects on oxygen vacancies in tantalum pentoxide. *J. Appl. Phys.* **2015**, *117*, No. 085308.
- (19) Kim, S.; Choi, S.; Lu, W. Comprehensive Physical Model of Dynamic Resistive Switching in an Oxide Memristor. *ACS Nano* **2014**, *8*, 2369–2376.
- (20) Kresse, G.; Hafner, J. Ab initio Molecular-Dynamics Simulation of the Liquid-Metal—Amorphous-Semiconductor Transition in Germanium. *Phys. Rev. B* **1994**, *49*, 14251—14269.
- (21) Freysoldt, C.; Grabowski, B.; Hickel, T.; Neugebauer, J.; Kresse, G.; Janotti, A.; Van de Walle, C. G. First-Principles Calculations for Point Defects in Solids. *Rev. Mod. Phys.* **2014**, *86*, 253–305.
- (22) Kamiya, K.; Yang, M. Y.; Magyari-Köpe, B.; Niwa, M.; Nishi, Y.; Shiraishi, K. Vacancy Cohesion-Isolation Phase Transition Upon Charge Injection and Removal in Binary Oxide-Based RRAM Filamentary-Type Switching. *IEEE Trans. Electron Devices* **2013**, *60*, 3400–3406.
- (23) Chen, J.-Y.; Huang, C.-W.; Chiu, C.-H.; Huang, Y.-T.; Wu, W.-W. Switching Kinetic of VCM-Based Memristor: Evolution and Positioning of Nanofilament. *Adv. Mater.* **2015**, *27*, 5028–5033.
- (24) Choi, S.; Lee, J.; Kim, S.; Lu, W. D. Retention Failure Analysis of Metal-Oxide Based Resistive Memory. *Appl. Phys. Lett.* **2014**, *105*, 113510–113516.
- (25) Wei, Z.; Kanzawa, Y.; Arita, K.; Katoh, Y.; Kawai, K.; Muraoka, S.; Mitani, S.; Fujii, S.; Katayama, K.; Iijima, M.; Mikawa, T.; Ninomiya, T.; Miyanaga, R.; Kawashima, Y.; Tsuji, K.; Himeno, A.; Okada, T.; Azuma, R.; Shimakawa, K.; Sugaya, H.; Takagi, T.; Yasuhara, R.; Horiba, K.; Kumigashira, H.; Oshima, M. Highly Reliable TaO_x ReRAM and Direct Evidence of Redox Reaction Mechanism. *IEEE Int. Electron Devices Meet.* 2008, 1–4.
- (26) Goldfarb, I.; Miao, F.; Yang, J. J.; Yi, W.; Strachan, J. P.; Zhang, M. X.; Pickett, M. D.; Medeiros-Ribeiro, G.; Williams, R. S. Electronic Structure and Transport Measurements of Amorphous Transition-Metal Oxides: Observation of Fermi Glass Behavior. *Appl. Phys. A* **2012**, *107*, 1–11.
- (27) Zhang, Y.; Wu, H.; Bai, Y.; Chen, A.; Yu, Z.; Zhang, J.; Qian, H. Study of Conduction and Switching Mechanisms in Al/AlO_x/WO_x/W Resistive Switching Memory for Multilevel Applications. *Appl. Phys. Lett.* **2013**, *102*, No. 233502.
- (28) Carrasco, J.; Lopez, N.; Illas, F. First Principles Analysis of the Stability and Diffusion of Oxygen Vacancies in Metal Oxides. *Phys. Rev. Lett.* **2004**, *93*, No. 225502.
- (29) Kim, Y. S.; Park, C. H. Rich Variety of Defects in ZnO via an Attractive Interaction between O Vacancies and Zn Interstitials: Origin of n-Type Doping. *Phys. Rev. Lett.* **2009**, *102*, No. 086403.
- (30) Lee, M.-J.; Lee, C. B.; Lee, D.; Lee, S. R.; Chang, M.; Hur, J. H.; Kim, Y. B.; Kim, C.-J.; Seo, D. H.; Seo, S.; Chung, U.-I.; Yoo, I.-K.; Kim, K. A Fast, High-Endurance and Scalable Non-Volatile Memory Device Made from Asymmetric Ta₂O_(5-X)/TaO_(2-X) Bilayer Structures. *Nat. Mater.* **2011**, *10*, 625–630.
- (31) Nakamura, R.; Toda, T.; Tsukui, S.; Tane, M.; Ishimaru, M.; Suzuki, T.; Nakajima, H. Diffusion of Oxygen in Amorphous Al₂O₃, Ta₂O₅, And Nb₂O₅. *J. Appl. Phys.* **2014**, *116*, No. 033504.
- (32) Li, Y.; Lei, Y.; Shen, B. G.; Sun, J. R. Visible-Light-Accelerated Oxygen Vacancy Migration in Strontium Titanate. *Sci. Rep.* **2015**, *5*, No. 14576.
- (33) Lee, J.; Lu, W.; Kioupakis, E. Electronic Properties of Tantalum Pentoxide Polymorphs from First-Principles Calculations. *Appl. Phys. Lett.* **2014**, *105*, No. 202108.
- (34) Lee, J.; Lu, W. D.; Kioupakis, E. Electronic and Optical Properties of Oxygen Vacancies in Amorphous Ta2O5 from First Principles. *Nanoscale* **2017**, *9*, 1120–1127.
- (35) Zhou, Y.; Yew, K. S.; Ang, D. S.; Kawashima, T.; Bera, M. K.; Zhang, H. Z.; Bersuker, G. White-Light-Induced Disruption of

- Nanoscale Conducting Filament in Hafnia. Appl. Phys. Lett. 2015, 107, No. 072107.
- (36) Zafar, S.; Jones, R. E.; Jiang, B.; White, B.; Chu, P.; Taylor, D.; Gillespie, S. Oxygen Vacancy Mobility Determined from Current Measurements in Thin Ba_{0.5}Sr_{0.5}TiO₃ Films. *Appl. Phys. Lett.* **1998**, *73*, 175–177.
- (37) Zafar, S.; Jagannathan, H.; Edge, L. F.; Gupta, D. Measurement of Oxygen Diffusion in Nanometer Scale HfO₂ Gate Dielectric Films. *Appl. Phys. Lett.* **2011**, *98*, No. 152903.
- (38) Jiang, H.; Stewart, D. A. Enhanced Oxygen Vacancy Diffusion in Ta₂O₅ Resistive Memory Devices due to Infinitely Adaptive Crystal Structure. *J. Appl. Phys.* **2016**, *119*, No. 134502.
- (39) Mikhaelashvili, V.; Betzer, Y.; Prudnikov, I.; Orenstein, M.; Ritter, D.; Eisenstein, G. Electrical Characteristics of Metal-Dielectric-Metal and Metal-Dielectric-Semiconductor Structures Based on Electron Beam Evaporated Y₂O₃, Ta₂O₅ and Al₂O₃ Thin Film. *J. Appl. Phys.* **1998**, *84*, 6747–6752.
- (40) Lau, W. S.; Leong, L. L.; Han, T.; Sandler, N. P. Detection of Oxygen Vacancy Defect States in Capacitors with Ultrathin Ta₂O₅ Films by Zero-Bias Thermally Stimulated Current Spectroscopy. *Appl. Phys. Lett.* **2003**, *83*, 2835–2837.
- (41) Perdew, J. P.; Burke, K.; Ernzerhof, M. Generalized Gradient Approximation Made. *Phys. Rev. Lett.* **1997**, 78 (7), 1396.